Resonant Cavity-Enhanced (RCE) Photodetectors

Katsumi Kishino, *Member, IEEE*, M. Selim Ünlü, *Student Member, IEEE*, Jen-Inn Chyi, J. Reed, L. Arsenault, and Hadis Morkoç, *Fellow, IEEE*

Abstract—**The photosensitivity characteristics of resonant cavity-enhanced (RCE) photodetectors have been investigated. The photodetectors were formed by integrating the active absorption region into a resonant cavity composed of top and bottom (buried) mirrors. A general expression for quantum efficiency η for RCE photodetectors was derived taking the external losses into account. Drastic enhancement in η is demonstrated at resonant wavelengths for a high quality factor Q cavity with a very thin absorption layer. An improvement by a factor of 4 in the bandwidth-efficiency product for RCE p-i-n detectors is predicted. Device parameters for achieving very high η (>0.99) without very thick absorption layers and any antireflection coating was discussed. Molecular beam epitaxially grown RCE-heterojunction phototransistors (RCE-HPT) were fabricated and measured demonstrating good agreement of the experiment and the theory. The wavelength selectivity of RCE detection was applied to wavelength demultiplexing. Crosstalk attenuation and efficiency-crosstalk product were calculated for various device parameters. Such a wavelength demultiplexing device was demonstrated by monolithically integrating three RCE-HPT's tuned at different wavelengths. The crosstalk attenuation was 12 dB.**

Introduction

HIGH SENSITIVITY photodetectors are crucial for optical communication, information, and sensing systems [1]–[3]. Various photodetectors, such as avalanche photodiodes, (APD) [2]–[4], p-i-n photodiodes (p-i-n PD) [3], [5], heterojunction phototransistors (HPT) [6]–[10], and metal-semiconductor-metal (MSM) photodiodes [11], [12] have been extensively studied. The quantum efficiency η of these conventional photodetectors, however, is basically limited by the absorption coefficient α, thickness d of the active layer, and surface reflection R, i.e., $\eta = (1 - R) \cdot (1 - e^{-\alpha d})$ [1]. So to achieve high η, a thick active layer along with antireflection coating is essential. For $\alpha = 10^4\ \mathrm{cm}^{-1}$, the quantum efficiency of a 1 μm thick absorber is limited to 63%, and to achieve $\eta > 95\%$ a very thick (>3 μm) active layer is required ($R = 0$). However, reduced device speed results from longer transit times required in such a device employing thick depletion region. Therefore, it is desirable to enhance the quantum efficiency without increasing the active layer thickness in order to optimize the gain-bandwidth product. This enhancement in η can be achieved by incorporating a multiple pass detection scheme, in which a single active layer serves many times in generating photocarriers.

Resonant cavity-enhanced (RCE) detectors having such a multiple-path detection scheme were demonstrated with AlGaAs–GaAs heterojunction phototransistors (HPT) [13], and with GaInAs–AlInAs Schottky photodiodes [14]. The former devices possess high quantum efficiences of 43% for a very thin active layer of only 0.1 μm. In this scheme, the detection region is integrated between two mirrors (top and bottom), and at the resonance condition, the incoming light interferes constructively with the reflected component from the bottom mirror. The resulting resonant cavity effect enhances the internal optical field amplitudes. For a high-quality factor Q cavity (high mirror reflectivities and thin absorption region) a drastic increase in η can be obtained. Therefore, a high η detection can be achieved even for a very thin (fractions of a micron or less) active layer.

We should note that this resonant cavity effect also provides wavelength selectivity of detection [13]. Therefore, RCE detectors can be viewed as high sensitivity detectors at selected wavelengths or monolithic integration of a detector with a filter. Hence, such detectors may also function as channel discriminators in wavelength division multiplexing system [15].

In the course of this paper, the general formulation of quantum efficiency of resonant cavity-enhanced (RCE) photodetectors is first presented. Then, fundamental properties of RCE detectors, such as quantum efficiency enhancement, wavelength-selectivity, incident light angle dependency of quantum efficiency, and high-speed response are theoretically discussed in detail. Using these considerations, the design concept and parameters of RCE detectors are given. The experimental results on AlGaAs–GaAs RCE-HPT's with an intermediate InGaAs layer in the collector are presented to demonstrate the RCE detection effect. Next, we discuss novel wavelength demultiplexing (WDM) devices, in which three RCE-HPT's with different resonant wavelengths are monolithically integrated. Here the RCE detection provides channel discrimination. Maximum crosstalk attenuation was 12 dB with an optical gain of 500. Finally, the channel crosstalk attenuation is discussed theoretically, and a performance figure of merit for these devices is devised in order to determine the optimum design structure.

Manuscript received October 23, 1990. This work was supported by the Office of Naval Research under Contract N00014-88-K-0724.

K. Kishino is with the Materials Research Laboratory and Coordinated Science Laboratory, University of Illinois, Urbana, IL 61801, on leave from Sophia University, Tokyo 102, Japan.

M. S. Ünlü, J.-I. Chyi, J. Reed, L. Arsenault, and H. Morkoç are with the Materials Research Laboratory and Coordinated Science Laboratory, University of Illinois, Urbana, IL 61801.

IEEE Log Number 9101359.

0018-9197/91/0800-2025$01.00 © 1991 IEEE

Enhanced Quantum Efficiency and High-Speed Properties for Resonant Cavity-Enhanced (RCE) Photodetectors

A. Formulation of Quantum Efficiency

First, an expression for the quantum efficiency of RCE photodectors will be formulated. Fig. 1 illustrates the model used in the analysis. Both of the end mirrors of the RCE photodetector may be made of quarter-wave stacks of semiconductor compounds or dielectric materials. For the top mirror, the native semiconductor to air interface can also be utilized, providing a reflectivity of approximately 30%, owing to the large refractive index difference at the boundary. The active layer thickness d and absorption coefficient α, where the photogeneration of carriers takes place, is between the two mirror structures. Distances to the active layer, from the top and the bottom mirrors, are symbolized by L_1 and L_2, respectively, and the absorption coefficient outside the active region is α_{ex}. Field reflection coefficients of the top and the bottom mirrors are $r_1 e^{-j\psi_1}$ and $r_2 e^{-j\psi_2}$, respectively, where ψ_1 and ψ_2 denote phase shifts due to light penetrating into the multiple-layer mirror region. Thus, the corresponding power reflectivity is $R_i = r_i^2$ $(i = 1, 2)$.

The electrical field component E_i of an incident light wave is transmitted into the detector as $t_1 \cdot E_i$. In the detector region the forward travelling field E_f is composed of this transmitted field and the feedback field reflected from the bottom mirror. Therefore, if the propagation constant is defined by β, the forward traveling wave E_f at $z = 0$ can be obtained through a self-consistent consideration, as

$$E_f = t_1 E_i + r_1 r_2 \, e^{-\alpha d - \alpha_{ex}(L_1 + L_2)} \, e^{-j(2\beta L + \psi_1 + \psi_2)} E_f \quad (1)$$

thus E_f is

$$E_f = \frac{t_1}{1 - r_1 r_2 \, e^{-\alpha d - \alpha_{ex}(L_1 + L_2)} \, e^{-j(2\beta L + \psi_1 + \psi_2)}} E_i. \quad (2)$$

Propagating E_f of (2) through the detector region, the backward traveling wave at $z = L$, E_b can be obtained as

$$E_b = r_2 e^{-\alpha d/2} \, e^{-\alpha_{ex}/2(L_1 + L_2)} \, e^{-j(\beta L + \psi_2)} E_f. \quad (3)$$

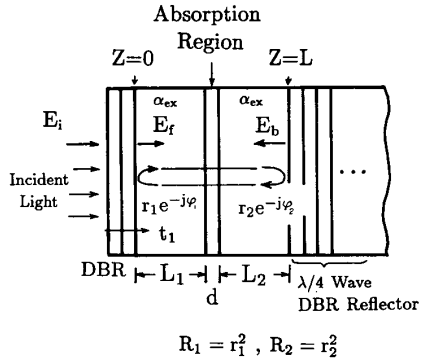

Fig. 1. Analysis model of resonant cavity enhanced (RCE) photodetectors.

The optical power inside the resonant cavity is given by

$$P_s = \frac{n}{2\eta_0} |E_s|^2 \qquad (s = f \text{ or } b) \quad (4)$$

where η_0 and n are the vacuum characteristic impedance of electromagnetic waves and the refractive index of the detector material, respectively.

In this case, the light power absorbed in the active layer (P_l) can be obtained in relation to the incident power P_i as

$$P_l = (P_f e^{-\alpha_{ex} L_1} + P_b e^{-\alpha_{ex} L_2})(1 - e^{-\alpha d}) = \frac{(1 - r_1^2)(e^{-\alpha_{ex} L_1} + r_2^2 e^{-\alpha_{ex} L_2} e^{-\alpha_c L})(1 - e^{-\alpha d})}{1 - 2 r_1 r_2 e^{-\alpha_c L} \cos(2\beta L + \psi_1 + \psi_2) + (r_1 r_2)^2 e^{-2\alpha_c L}} P_i \quad (5)$$

Thus, the quantum efficiency η is given by

$$\eta = \left\{ \frac{(e^{-\alpha_{ex} L_1} + e^{-\alpha_{ex} L_2} R_2 e^{-\alpha_c L})}{1 - 2\sqrt{R_1 R_2} e^{-\alpha_c L} \cos(2\beta L + \psi_1 + \psi_2) + R_1 R_2 e^{-2\alpha_c L}} \right\} \times (1 - R_1)(1 - e^{-\alpha d}) \quad (6)$$

where α_c is

$$\alpha_c = (\alpha_{ex} L_1 + \alpha_{ex} L_2 + \alpha d)/L. \quad (7)$$

Since α_{ex} is usually around 5–10 cm^{-1}, i.e., small compared to the absorption coefficient of the active layer, α $(\geq 10^4$ $cm^{-1})$, we can neglect α_{ex} in (6), except for the case of an extremely thin active layer or extremely thick external layer. Thus η is

$$\eta = \left\{ \frac{(1 + R_2 e^{-\alpha d})}{1 - 2\sqrt{R_1 R_2} e^{-\alpha d} \cos(2\beta L + \psi_1 + \psi_2) + R_1 R_2 e^{-2\alpha d}} \right\} \times (1 - R_1)(1 - e^{-\alpha d}) \quad (8)$$

where $\beta = 2n\pi/\lambda$ (λ: wavelength and n: refractive index).

The above quantum efficiency is a periodic function of the inverse wavelength. Fig. 2 shows the calculated wavelength dependency of η where three curves for $R_1 =$ 0.9, 0.3, and 0.05 are drawn assuming $R_2 = 0.9$, $\alpha d =$ 0.1, and $L = 2$ μm. We note here that the quantum efficiency is enhanced periodically at the resonant points determined by $2\beta L + \psi_1 + \psi_2 = 2m\pi$ $(m = 1, 2, 3, \cdots)$.

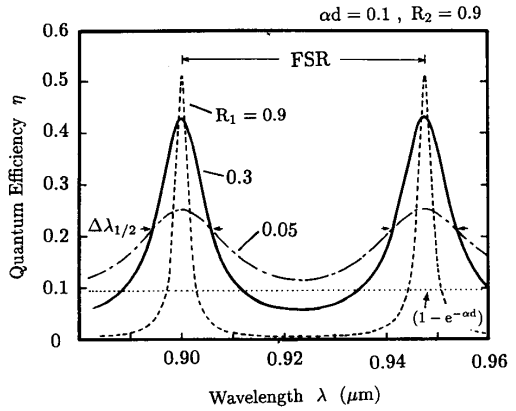

Fig. 2. Wavelength dependency of the quantum efficiency for RCE detectors for various top mirror reflectivities $R_1 = 0.05$, 0.3, and 0.9, respectively, at absorption parameter $\alpha d = 0.1$ and the bottom mirror reflectivity $R_2 = 0.9$.

The dotted line in Fig. 2 indicates the value given by $1 - e^{-\alpha d}$, the maximum η value attainable for a conventional photodetector.

On the right-hand side of (8), the term inside the brackets gives the cavity enhancement effect. This term becomes unity when $R_2 = 0$ giving the quantum efficiency for a conventional detector without the cavity structure, i.e., $\eta = (1 - R_1)(1 - e^{-\alpha d})$.

In the above derivation of (8), the standing wave effect in the cavity was not taken into account. This could lead to inaccuracies for very thin absorbing layers having thicknesses significantly below that of the standing wave period. This discrepancy can be accounted for within this model by introducing an α_{eff} to replace α.

The peak quantum efficiency at resonant points η_p is from (8):

$$\eta_p = \left\{\frac{(1 + R_2 e^{-\alpha d})}{(1 - \sqrt{R_1 R_2}\, e^{-\alpha d})^2}\right\} \times (1 - R_1)(1 - e^{-\alpha d}) \quad (9)$$

and in the limit of a thin active layer, i.e., $\alpha d \ll 1$, η_p is

$$\eta_p \simeq \left\{\frac{(1 + R_2(1 - \alpha d))}{(1 - \sqrt{R_1 R_2}(1 - \alpha d)^2}\right\} \times (1 - R_1)\alpha d. \quad (10)$$

At the off-resonance points, that is when $2\beta L + \psi_1 + \psi_2 = (2m + 1)\pi (m = 1, 2, 3, \cdots)$, the field amplitude of the light between the two end mirrors decreases due to the destructive interference of forward and backward travelling waves, resulting in suppressed quantum efficiency as shown in Fig. 2. The wavelength spacing between neighboring resonant peaks, i.e., free spectral range (FSR), can be expressed as

$$\text{FSR} = \frac{\lambda^2}{2n_{\text{eff}}(L + L_{\text{eff},1} + L_{\text{eff},2})} \quad (11)$$

where n_{eff} is the effective refractive index, and $L_{\text{eff},i}$ are the effective optical length of the multi-layer mirrors. Generally, $L_{\text{eff},i}$ can be given by [16]

$$L_{\text{eff},i} = \frac{1}{2}\frac{\partial \psi_i}{\partial \beta} (i = 1, 2). \quad (12)$$

An experimental example of the L_{eff} value for a GaAs–AlGaAs stacked layer mirror is 0.7 μm, found by adding two effective lengths on both the top (five periods) and bottom (eight and a half periods) mirrors [17].

The ratio of FSR to the wavelength full width at half maximum $\Delta\lambda_{1/2}$ is a measure of the wavelength selectivity of detection. This ratio is usually referred to as finesse F, and can be derived from (8) as follows:

$$F = \frac{\text{FSR}}{\Delta\lambda_{1/2}} = \frac{\pi (R_1 R_2)^{1/4} e^{-\alpha d/2}}{1 - \sqrt{R_1 R_2}\, e^{-\alpha d}}. \quad (13)$$

B. Quantum Efficiency Enhancement by Resonant Cavity Effect

The origin of such drastic enhancements of quantum efficiency is the enhanced amplitude of the internal field inside a high Q resonant cavity. This amplitude enhancement can be evaluated by the internal optical power increment factor to the incident power defined by $(P_f + P_b)/P_i$. This factor is identical to the right hand term of the quantum efficiency in (8) except for $(1 - e^{-\alpha d})$ term, and therefore, it expresses the absolute improvement of quantum efficiency by the cavity effect over an idealized conventional detector ($R_1 = R_2 = 0$) with the same active layer thickness.

The internal optical power increment factor at resonance for $R_1 = 0.3$, 0.7, and 0.9, with $R_2 = 0.99$ and 0.90 was calculated neglecting the external absorption α_{ex}. Fig. 3 shows the calculated results as a function of normalized absorption coefficient αd where solid lines are for $R_2 = 0.99$ and dotted lines for $R_2 = 0.90$. For small αd, i.e., low loss cavity, the increment factor exceeds 10 and can reach 50 or more at the higher top and bottom mirror reflectivities resulting in a reasonably high quantum efficiency even for a thin active layer. Here, the internal optical power can be greatly enhanced by increasing the front and bottom mirror reflectivites. On the other hand, with increasing αd, this increment factor decreases rapidly, especially for the high Q cavity (e.g., $R_1 = 0.9$ and $R_2 = 0.99$), and becomes less than unity.

Multiplying the internal optical power increment factor of the resonant cavity by $(1 - e^{-\alpha d})$ results in quantum efficiency η of RCE photodetectors (8). Fig. 4 shows η at resonant modes as a function of αd (or thickness in microns for $\alpha = 10^4\ \text{cm}^{-1}$) for variance R_1 values and $R_2 = 0.9$ (solid lines). The η for the no reflector case ($R_2 = 0$) is also given by a dotted–dashed line and η for $R_1 = 0.7$, $R_2 = 0.99$ is shown by a dashed line. When the two curves of $R_2 = 0$ and 0.9 for $R_1 = 0.3$ are compared to each

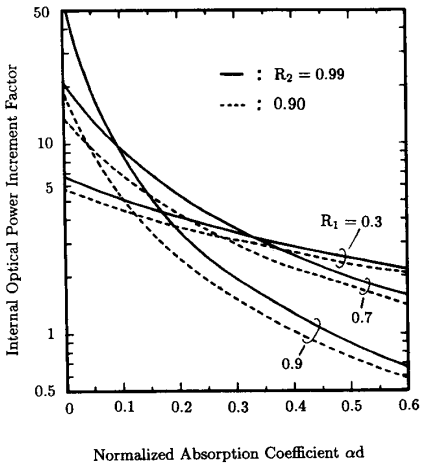

Fig. 3. Internal optical power increment factor in resonant cavities with various end mirror reflectivities as a function of the normalized absorption coefficient αd.

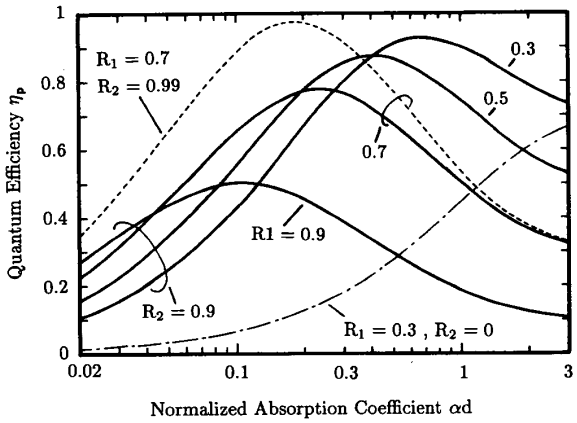

Fig. 4. Calculated quantum efficiency versus αd. Solid lines show η at the resonance mode peaks for $R_2 = 0.9$, a dashed line for $R_2 = 0.99$ and $R_1 = 0.7$, and dotted-dashed line shows the no reflector case ($R_2 = 0$, $R_1 = 0.3$).

other, we notice that the cavity enhancement improves η from 6.7 to 43% (a factor of 6.5) for 0.1 μm thick absorption layer ($\alpha = 10^4$ cm^{-1}). Even higher quantum efficiency can be obtained by increasing the bottom mirror reflectivity. For example, when $R_2 = 0.99$ as $R_1 = 0.7$, a maixmum η in excess of 98% can be expected as shown in Fig. 4.

The absorption term $(1 - e^{-\alpha d})$ increases with increasing αd, while the internal power increment factor decreases as shown in Fig. 3. Therefore, η is a maximum at a certain αd and decreases with increasing thickness to the conventional value determined by the top mirror reflectivity, i.e., $\eta_{d\to\infty} = 1 - R_1$. For a thick absorption region, most of the light is absorbed before it reaches the bottom mirror. Thus, the feedback mechanism, i.e., the cavity effect is removed.

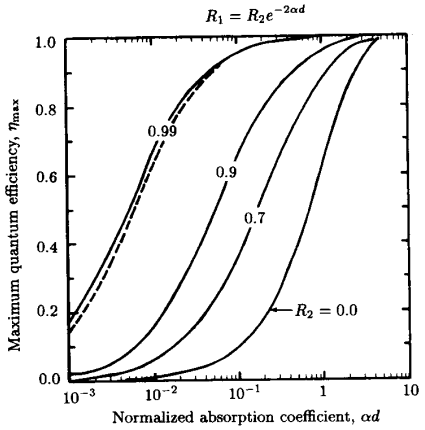

Fig. 5. Maximized quantum efficency versus αd. The maximizing condition is $R_1 = R_2 e^{-2\alpha d}$. Dashed lines show η for $\alpha_{ex} L_1 = \alpha_{ex} L_2 = 5 \times 10^{-4}$ (i.e., $\alpha_{ex} = 5$ cm^{-1}, $L_1 = L_2 = 1$ μm).

From (9), the quantum efficiency at a certain αd value is maximized when $R_1 = R_2 e^{-2\alpha d}$. Fig. 5 shows the maximum η as a function of αd for various R_2 values. For conventional detectors without the cavity effect, high quantum efficiency (>90%) can be realized only for a thick active layer of more than 2–3 μm (see the curve for $R_2 = 0$ in Fig. 5). In the case of RCE photodetectors, however, when $R_2 = 0.99$, a maximum quantum efficiency exceeding 90% can be easily realized for very thin active layers of 0.04–0.05 μm thickness ($\alpha = 10^4$ cm^{-1}) as shown in Fig. 5. This fact is very helpful towards improving the high-speed performance of detectors because the electronic transit time along the depletion absorption region may eventually govern the high-frequency performance. The high-speed behavior of RCE detectors will be discussed later.

When the αd value is very small, the effect of α_{ex} may not be neglected. The dashed line in Fig. 5 represents η for $\alpha_{ex} = 5$ cm^{-1} and $L_1 = L_2 = 1$ μm. A small discrepancy from the lossless cavity results ($\alpha_{ex} = 0$) is observed only for $R_2 = 0.99$ in the case of small αd. For practical αd values, however, this discrepancy is negligibly small.

From the above discussion, it is understood that high quantum efficiency photodetectors with $\eta > 99\%$ can be realized for a thin absorption region, but at the expense of their wide spectral photosensitivity performance. Fig. 6 shows the constant η contours as a function of top mirror reflectivity R_1 and normalized absorption coefficient αd. The parameter region of R_1 and αd as $R_2 = 0.99$ for getting $\eta > 99\%$ is indicated by the meshed region. For $\eta > 99\%$ with $R_1 = 0.2$, a deviation of absorption thickness d from 0.7 to 0.95 μm at $\alpha = 10^4$ cm^{-1} is allowed. Similarly, high η can be obtained for a range of top mirror reflectivities. For example, at $\alpha d = 0.7$, $\eta \geq 0.99$ range extends from $R_1 = 0.2$ to $R_1 = 0.3$ (native GaAs surface).

A conventional detector, although it has a wide-range flat sensitivity, requires a very thick absorption layer in excess of 5 μm, to absorb 99% of the incoming light even

with a perfect antireflection coating. The secondary recombination of photo-generated carriers while drifting through such a thick depletion region will then limit η introducing an additional difficulty for achieving very high η (>99%). In the case of RCE detectors, achieving high η detection at a single wavelength is easier, but tuning the wavelength may be necessary. However, wavelength tuning can be carried out by recessing the surface as described below [13].

C. Angle Dependency of Quantum Efficiency

Quantum efficiencies of RCE photodetectors given by (6)–(9) are for the normal incidence of incoming light. The expression of η for off-angle incoming light with an incident angle θ_i can be obtained by replacing β with $\beta \cos\theta$ in (6) and (8). Here, by Snell's law, $n \sin\theta = \sin\theta_i$, and also note that ψ_i ($i = 1, 2$) is a function of β. When the incident angle is shifted from the normal, the peak value of quantum efficiency η_p (Fig. 4) will decrease since the resultant change in the optical path length causes a shift from the resonance wavelength. Here the new resonance wavelength should be determined by $2\beta \cos\theta = 2m\pi$. Thus, for small θ_i, the relation of the wavelength shift $\Delta\lambda$ to the incident angle is approximately

$$|\Delta\lambda| \sim \frac{1}{2}\left(\frac{\theta_i}{n}\right)^2 \lambda. \tag{14}$$

From the wavelength dependent equation of η (8) and the above equation (14), the angle dependency of η can be obtained as a function of the cavity finesse F, wavelength λ, cavity length L, effective refractive index n_{eff}, and refractive index n, as follows:

$$\frac{\Delta\eta}{\eta} = \frac{\eta_p - \eta}{\eta} = \left[\frac{2n_{\text{eff}}(L + L_{\text{eff},1} + L_{\text{eff},2})}{\lambda} F\left(\frac{\theta_i}{n}\right)^2\right]^2. \tag{15}$$

Equation (15) indicates that η is most sensitive to the angle of incidence for a high finesse cavity at shorter wavelengths. Although this behavior may be very useful for special applications (such as high response angle detection), it becomes a drawback for RCE detectors in many applications. However, this drawback can be practically overcome. As shown in Fig. 7, η does not change appreciably within the incident angle 5° even for very high-finesse cavities with $F = 10$ and 20 at the wavelengths of 1 and 1.5 μm. For lower finesse cavities, this angle condition can be relaxed, still keeping the benefit of resonant cavity effect. A light beam can be aligned easily within 5°, and if the detector modules fixed with fiber coupler and microlens is utilized, the induced detection instability due to shocks may be completely eliminated. Furthermore, when the RCE detection scheme is integrated into optoelectronic circuits, a good light beam alignment can be obtained by a simple arrangement of devices.

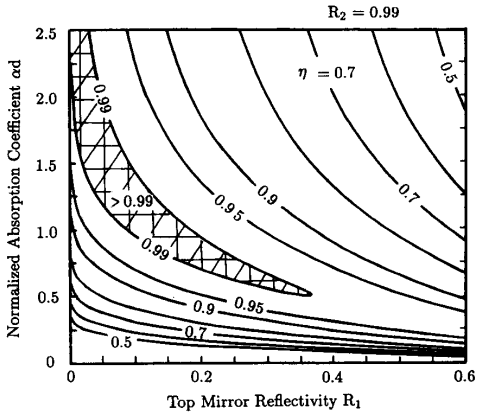

Fig. 6. Relation between the absorption coefficient αd and the top mirror reflectivity R_1 as $R_2 = 0.99$ for a constant quantum efficiency. Quantum efficiency greater that 0.99 can be obtained in the meshed region.

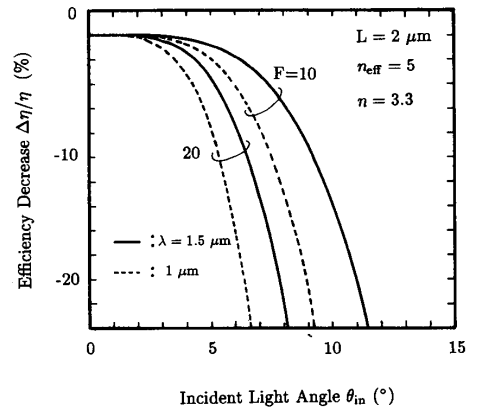

Fig. 7. Incident light angle dependency of the quantum efficiency for the high finesse cavity with $F = 10$ and 20 at wavelengths of 1 and 1.5 μm.

D. High-Speed Response Properties

High-speed response of a simple photodetector (e.g., p-i-n, MSM detectors) is restricted chiefly by the transit time through the depletion layer and the device capacitance (i.e., *RC* time constant). The RCE scheme provides a high η detection for a thin active layer. The transit time limited 3 dB bandwidth of a thin p-i-n detector f_v is approximately [18]

$$f_v = 0.45\left(\frac{v}{d}\right) \tag{16}$$

where v is the carrier velocity (for simplicity equal electron and hole velocities are assumed).

The bandwidth-efficiency product $f_v \cdot \eta$ calculated from (9) and (16) is shown in Fig. 8, for $R_2 = 0.9$ where the curves for $R_1 = 0.3$ and 0.9 are given by solid and dotted–dashed lines, respectively. For thin active layers, the *RC* time limited product $f_{\text{RC}} \cdot \eta$ restricts the high speed performance dependent on the device size ($R = 50\ \Omega$). The

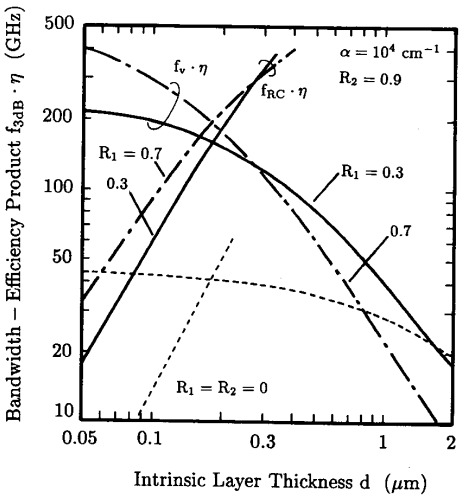

Fig. 8. Bandwidth-efficiency product versus active layer thickness d of RCE photodetectors, where $\alpha = 10^4$ cm^{-1}, $R_2 = 0.9$. Solid and dotted-dashed lines show $f_{3dB} \cdot \eta$ of RCE photodetectors, and dashed lines a conventional detector without cavity. $f_v \cdot \eta$ is the transit time limited product and $f_{RC} \cdot \eta$ the RC time limited product.

dashed line indicates the bandwidth-efficiency product for a conventional idealized photodetector (i.e., $R_1 = R_2 = 0$). As a result, we note that the high-speed detection ability can be enhanced very much by the RCE effect, here by a factor of 4. For RCE detectors with low capacitance, e.g., MSM detectors [11], [12], the RC time limit may be relaxed and ultrahigh-speed detection can be obtained.

Resonant Cavity Enhanced AlGaAs–GaAs Heterojunction Phototransistors

Resonant cavity enhanced (RCE) detection can also be realized for AlGaAs–GaAs heterojunction phototransistors (HPT's) using an intermediate smaller bandgap (InGaAs) collector layer [13]. Fig. 9 shows the layer structure of AlGaAs–GaAs RCE-HPT where the resonant cavity is formed between the embedded quarter-wave stack bottom mirror and the epitaxial layer surface. By introducing the InGaAs layer, the photosensitivity spectrum extends to longer wavelengths (>900 nm) where the absorption in the base and the heavily doped GaAs collector is negligible. Having a lossless structure, except for the thin active region, enables the formation of a high quality factor Q cavity. The estimated Q of the cavity for lossless case is about 75 at $\lambda = 900$ nm. The measured Q with a 0.1 μm InGaAs absorbing layer is 60 which is only 20% shy of the lossless case.

The RCE-HPT's were grown by molecular beam epitaxy (MBE) initiating with a 0.5 μm n$^+$-GaAs buffer layer on an (100) n-GaAs substrate. This was followed by a ten pair AlAs–GaAs high reflectivity mirror ($R = 0.9$, center wavelength 950 nm). After the mirror, the HPT contains, successively from the substrate side, a 0.5 μm n$^+$-GaAs subcollector, a 0.4 μm n-GaAs collector ($n = 5 \times 10^{16}$ cm^{-3}) and a 0.1 μm undoped $In_{0.05}Ga_{0.95}As$ collector, a p-GaAs base (0.1 μm, $p = 5 \times 10^{17}$ cm^{-3}) and a n-$Al_{0.3}Ga_{0.7}As$ emitter (0.2 μm $n = 5 \times 10^{17}$ cm^{-3}), and finally, a 0.1 μm AlGaAs and a 500 Å GaAS cap layers (both $n = 5 \times 10^{18}$ cm^{-3}). For the reference, a conventional HPT with identical structure without the bottom mirror was also grown. After growth, 300 μm circular HPT's with 250 μm windows were fabricated. The photosensitivity of the fabricated devices was evaluated under the illuminaton of a monochromatic light source with a spot size of 500 μm. The spectrum of this source was calibrated by a Si-detector.

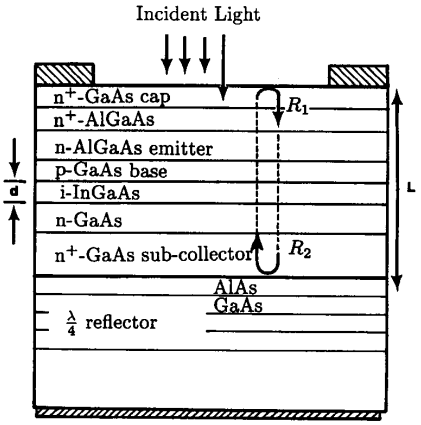

Fig. 9. Schematic layer structure of the investigated RCE-HPT's.

The wavelength spectrum of the photosensitivity of the RCE-HPT is shown in Fig. 10 by the dashed line, in comparison to that of the conventional HPT (solid line). The latter spectral response was cut sharply around the band-edge wavelength of GaAs at 860 nm, with a small increase at around 900 nm which was solely due to absorption in the InGaAs layer. The cavity loss should be very low at 900 nm so it follows that the sensitivity of the HPT at longer wavelengths was limited by the thickness of the InGaAs region, i.e., 0.1 μm, for conventional HPT. Under pulsed laser illumination, the optical gain of the HPT was measured to be above 500 at 850 nm (calculated η = 25%) and 150 at 900 nm (InGaAs region absorption wavelength, η = 6.7%) at $V_{ce} = 5$ V and $I_c = 30$ mA [13]. The dark current measured for a 250 μ device was 5 pA (1×10^{-8} A/cm^2).

On the other hand, the photosensitivity of the RCE-HPT with a resonant cavity formed between a buried mirror structure and the epilayer surface was greatly enhanced at certain wavelengths, as shown in Fig. 10. At the resonant peak of 900 nm, where the low-loss cavity was realized, the detected current increased to seven times of the HPT without reflectors. This resonant cavity enhancement almost coincides with the theoretical enhancement factor of 6.5 for the same reflectivities and active layer thickness, as discussed previously in Fig. 4. The increase at 850 nm was only a factor of 1.7. Here, the two spectral responses

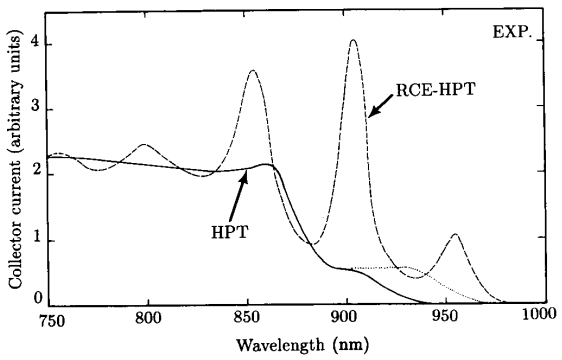

Fig. 10. Spectral response of floating base HPT's, i) without reflectors (solid line) and ii) with resonant cavity enhancement (dashed line). The dotted line shows the estimated spectrum for the latter when the cavity influence is removed. Note that the band edge of the InGaAs region moves to longer wavelengths due to inaccuracy in the In-mode fraction.

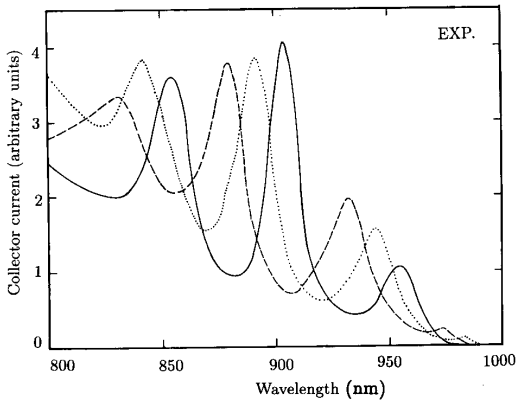

Fig. 11. The spectral response of RCE-HPT as the surface is thinned: i) as-grown (solid), ii) etched 350 Å (dotted), and iii) etched 600 Å (dashed).

were normalized at 750 nm where the cavity effect is negligible.

From Fig. 10 we observe that the RCE-HPT yielded a smaller enhancement of the photosensitivity at 850 nm (absorption in 0.5 μm InGaAs–GaAs collector) compared to 900 nm (absorption in 0.1 μm InGaAs) resulting in almost identical sensitivities at these two wavelengths in contrast with the drastic difference in the thickness of the active absorption region. Absorption losses in the base and subcollector in addition to larger absorption by thicker active collector layers (total lossy region 1.15 μ) degrades the cavity enhancement effect at 850 nm as predicted theoretically. At 850 nm, a cavity enhancement factor is calculated to be 1.8 which is in very good agreement with the experimental value of 1.7. Note that in Fig. 10 the sensitivity between the resonance peaks is below that of the conventional HPT without reflectors, owing to the incident light at off-resonance wavelengths being rejected from the cavity. The calculated finesse of a cavity with reflectivities of $R_1 = 0.3$ and $R_2 = 0.9$ and a 0.1 μm thick absorbing region is 4 from (13), which is in good agreement with the experimental value of 3.6 as obtained from Fig. 10.

As described previously, the peak quantum efficiency of RCE-HPT's at resonance points can be maximized at a certain top mirror reflectivity ($R_1 = R_2 \cdot e^{-\alpha d}$). For example, for $R_2 = 0.9$ and $\alpha d = 0.1$, a maximum $\eta = 65\%$ can be obtained at $R_1 = 0.74$. To obtain such a high surface reflectivity, however, it is required that an additional reflector structure grown above the active device. Furthermore, with this reflector the cavity length and in turn the resonance modes will be fixed.

Fortunately, regrowth process of the top mirror enables the cavity modes to be tuned to any desired wavelength. In this process, a top mirror dielectric or semiconductor layers can be grown after the resonant wavelength is tuned simply by recessing the surface for changing the cavity length. Tuning by surface etching is demonstrated in Fig. 11 where spectral responses of RCE-HPT's of the as-grown structure (solid line) and after etching the cap layer approximately 350 Å (dashed) and 600 Å (dotted) are given.

As a result, high gain and very fast detectors with high quantum efficiencies, at a variety of selected wavelengths can be fabricated on the same wafer. Thus, the RCE-HPT may also function as a wavelength demultiplexing device for wavelength division multiplexing (WDM) systems [15].

Wavelength Demultiplexing Function of RCE Photodetectors

Wavelength division multiplexing (WDM) is a key technology for increasing the transmission capacity of optical fiber communication systems. In this system a high-speed and high-gain demultiplexing receiver is a crucial part of the system performance [19]–[22].

A wavelength demultiplexing detector using RCE-HPT's can be composed as shown in Fig. 12 where, as an example, four RCE-HPT's with the different resonance wavelengths are monolithically integrated [23]. Each RCE-HPT can function as a channel discriminator for picking up the corresponding channel signal from the common incoming light beam among the detectors. For this device scheme, the detected photocurrent of individual detectors will decrease by sharing the light power, but high phototransistor gain will compensate for this. This type of device can provide a very simple but effective wavelength demultiplexing detection scheme, especially for small channel number demultiplexing or short distance WDM communication systems.

As described above, the resonance wavelength of the cavity can be tuned by recessing the epitaxial layer surface, i.e., changing the cavity length L. In the demultiplexing detector depicted in Fig. 12, four RCE-HPT's with different cavity lengths (L_1 through L_4) provide different resonant wavelengths (1 through 4).

The very prototype of such a wavelength demultiplex-

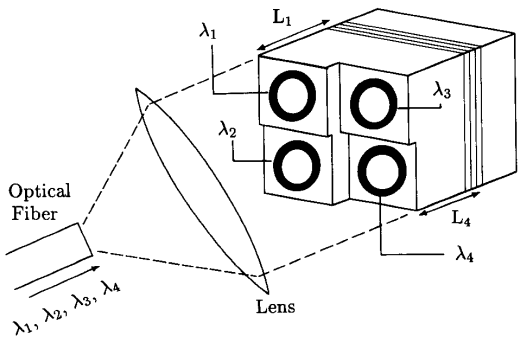

Fig. 12. Conceptual diagram of an application for the demultiplexing detector composed for the four RCE-HPT's with different resonance wavelengths.

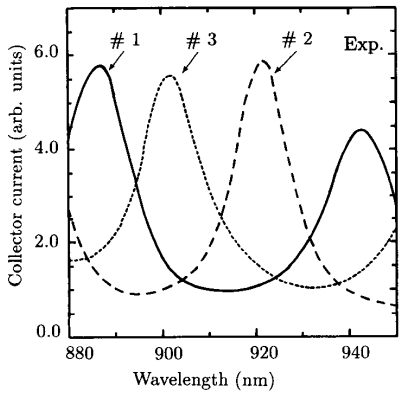

Fig. 13. Spectral response of the three devices with different surface recessing depicted in Fig. 12. The portion of the wavelength spectrum over one free spectral range with minimum crosstalk is shown.

ing detector was fabricated using the same RCE-HPT structure discussed above. Standard photolitohgraphic techniques were employed to fabricate 300 μm circular RCE-HPT's with 250 μm windows. The demultiplexing receiver structure was formed by selective recessing of the window surfaces of neighboring devices by 350, 700, and 1050 Å. In this study, the surface recessing was adjusted to obtain only three equally spaced modes to achieve high crosstalk attenuation. Therefore, the spectral response of device #4 was identical to that of device #1.

Fig. 13 shows the spectral responses of devices 1–3 under equal illumination and a collector emitter bias of 3 V. The free spectral range (FSR) of the device was around 55 nm at 900 nm center wavelength and full width at half maximum (FWHM) $\Delta\lambda_{1/2}$ was 15 nm with a resulting finesse F of 3.6. The maximum crosstalk attenuation for dual wavelength demultiplexing was demonstrated to be over 15 dB. For three wavelength demultiplexing, the crosstalk attenuation is around 12 dB, slightly less than the theoretical value of 15.6 dB for $F = 3.6$ and $N = 3$.

Using the wavelength dependent quantum efficiency equation for RCE detectors (8), the interchannel crosstalk attenuation (C) can be derived approximately as a function of finesse and number of channels (N) as

$$C \simeq 20 \log \left[1 + \left(\frac{2F}{N}\right)^2\right] \quad (N > 3) \qquad (17)$$

where the finesse is given by (13) in relation to mirror reflectivities R_1, R_2, absorbing layer thickness d, and the absorption coefficient α.

From (17), we note that a very high crosstalk attenuation can be obtained for a very high finesse cavity formed by increasing the end mirror reflectivities for a thin absorption layer as shown in Fig. 14. For example, when $\alpha d = 0.01$ and $\alpha_{ex} = 0$, a finesse value as large as 100 can be expected for end mirror reflectivities of $R_2 = 0.99$ and $R_1 = 0.985$. The performance of wavelength demultiplexing detectors is evaluated by the figure of merit defined by the product $\eta \cdot C$. We calculated the product $\eta \cdot C$ as a function of αd, assuming the maximized η condition ($R_1 = R_2 e^{-2\alpha d}$) and four-channel demultiplexing,

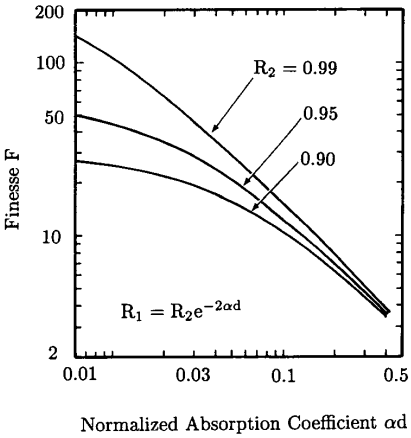

Fig. 14. Cavity finesse of maximized η RCE-detectors as a function of αd.

as shown in Fig. 15. Examining (17) and the finesse dependency on αd (Fig. 14), we note that C should increase monotonically with decreasing αd. But as η decreases at the small αd region as shown in Fig. 5, the product $\eta \cdot C$ peaks at a certain value of αd. Thus, a high performance demultiplexing detector can be obtained in the region around $\alpha d = 0.1$ or less for higher R_2. For an absorption layer thickness of 0.1 μm (i.e., $\alpha d = 0.1$), dependencies of each C and η on the mirror reflectivities are sown in Fig. 16.

In the above prototype device, the buried mirror is only ten periods with a corresponding peak reflectivity of $R_2 = 90\%$ and the top mirror is the epilayer surface with $R_1 = 30\%$. Increasing the number of periods for the bottom mirror to 15 will result in 99% peak reflectivity and enhance the wavelength selectivity. Therefore, a drastic improvement of demultiplexing performance can be achieved by increasing the front and bottom mirror reflectivities. For example, when $R_1 = 0.90$, $R_2 = 0.99$ and $\alpha d = 0.1$, F is 20, resulting in crosstalk attenuation values of 24 dB

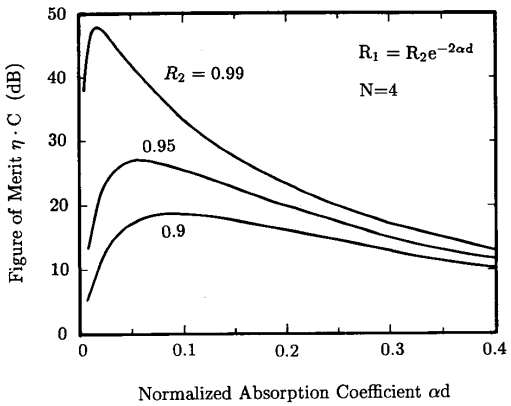

Fig. 15. The quantum efficiency-crosstalk attenuation product (figure of merit) $\eta_c \cdot C$ for wavelength demultiplexing RCE detectors versus αd for four channel demultiplexing ($N = 4$).

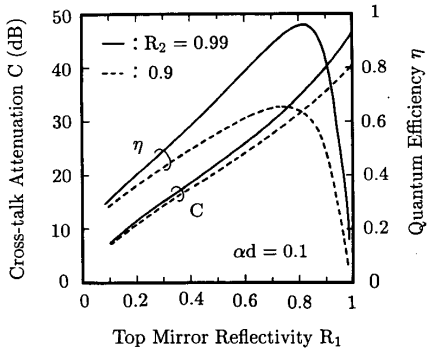

Fig. 16. Crosstalk attenuation and quantum efficiency of the investigated wavelength demultiplexing detector as a function of the top mirror reflectivity. The solid line shows η and C for $R_2 = 0.99$ and the dashed line for $R_2 = 0.9$.

and 40 dB for ten- and four-channel demultiplexing, respectively, while η is 85%.

Note that with increasing F, wavelength FWHM $\Delta\lambda_{1/2}$ will decrease enabling the reduction of interchannel wavelength spacing ($F = 20$, gives $\Delta\lambda_{1/2} < 3$ nm for the investigated structure). Therefore, with improving wavelength selectivity the number of demultiplexing wavelengths within the same FSR can be increased.

Conclusion

The photosensitivity characteristics of resonant cavity enhanced (RCE) photodetectors has been investigated. The photodetectors were formed by integrating the active absorption region into a resonant cavity composed by top and bottom mirrors. A general expression of the quantum efficiency η for RCE photodetectors was derived taking the external layer losses into account for the first time. Using this equation, various detection properties of RCE photodetectors were discussed giving the following results:

i) Under the resonance condition, the enhanced amplitude of internal optical fields results in drastic increases in absorption and thus η. Since off-resonance wavelengths are rejected from the cavity, RCE photodetectors can also provide wavelength selectivity. Therefore, an array of RCE-HPT's tuned at different wavelengths can be used as a wavelength demultiplexing receiver.

ii) Using a low-loss, high-Q cavity, reasonably high photosensitivities can be achieved for very thin active layers. Consequently, as a result of relaxing the transit time limit on the high speed performance, the bandwidth-efficiency product can be enhanced by a factor of 4.

iii) The resonant cavity effect can also be used in obtaining very high quantum efficiencies ($\eta \simeq 1.0$) at selected wavelengths, without requiring very thick absorbing layers or anti-reflection coating. For example, $R_2 = 0.99$ and $\alpha d = 0.6$ ($d = 0.6$ μm as $\alpha = 10^4$ cm^{-1}) give $\eta > 0.99$ for native semiconductor surface (GaAs: $R_1 \simeq 0.3$) at the resonant wavelength. This resonant wavelength can be tuned by recessing the surface.

iv) Quantum efficiency η is most sensitive to the incident angle of incoming light for a high finesse cavity at shorter wavelength. But η does not appreciably change within the 5° or normal incidence even for very high finesse of $F = 10$-20 for $\lambda = 1$-1.5 μm.

In brief, the detection mechanism of RCE photodetectors was discussed in detail in relation to device parameters such as reflectivities and absorption coefficients, giving us the basic tools for designing these devices for various applications.

To demonstrate the theoretical results, AlGaAs–GaAs RCE-HPT's with an InGaAs intermediate collector layer were grown and fabricated. The measured enhancement in η was in good agreement with calculations.

A monolithic three wavelength demultiplexing receiver was formed by integrating three RCE-HPT's tuned at different wavelengths. The demultiplexing ability of RCE detection scheme predicted theoretically was therefore confirmed. A crosstalk attenuation of 12 dB was obtained. The crosstalk attenuation and the efficiency-crosstalk product were calculated for various end mirror reflectivities and the absorption coefficient αd. A figure of merit for optimum device design was discussed.

References

[1] H. David Law, *Semiconductors and Semimetals, Lightwave Communication Technology*, W. T. Tsang, Ed. New York: Academic, 1985, vol. 22, part D, p. 454.

[2] H. D. Law, K. Nakano, and L. R. Tomasetta, "III-V alloy heterostructure high speed avalanche photodiodes," *IEEE J. Quantum Electron.*, vol. QE-15, pp. 549-558, 1979.

[3] T. P. Pearsall, "$Ga_{0.47}In_{0.53}As$: A ternary semiconductor for photodetector applications," *IEEE J. Quantum Electron.*, vol. QE-16, pp. 709-720, 1980.

[4] N. Susa, H. Nakagome, H. Ando, and H. Kanabe, "Characteristics in InGaAs/InP avalanche photodiodes with separated absorption and multiplication regions," *IEEE J. Quantum Electron.*, vol. QE-17, pp. 243-249, 1981.

[5] T. P. Lee, C. A. Burrus, Jr., and A. G. Dentai, "InGaAs/InP p-i-n photodiodes for lightwave communications at the 0.95-1.65 μm

wavelength," *IEEE J. Quantum Electron.*, vol. QE-17, pp. 232-238, 1981.
[6] J. C. Campbell, A. G. Dentai, C. A. Burrus, Jr., and J. F. Ferguson, "InP/InGaAs heterojunction Phototransistors," *IEEE J. Quantum Electron.*, vol. QE-17, pp. 264-269, 1981.
[7] F. Capasso, W. T. Tsang, C. G. Bethea, A. L. Hutchinson, and B. F. Levine, "New Graded band-gap picosecond Phototransistor," *Appl. Phys. Lett.*, vol. 42, p. 93, 1983.
[8] N. Chand, J. Klem, and H. Morkoç, "Pnp GaAs/Ge/Ge phototransistor grown by molecular beam epitaxy: Implications for bipolar and hot electron transistors," *Appl. Phys. Lett.*, vol. 48, pp. 484-486, 1986.
[9] J. K. Twyham, P. A. Claxton, R. C. Woods, and D. R. Wright, "High-gain GaInP/GaAs heterojunction phototransistor utilizing guard ring structure," *Electron Lett.*, vol. 25, pp. 86-87, 1989.
[10] J. C. Campbell, W. T. Tsang, and G. L. Qua, "$InP/In_{0.53}Ga_{0.47}As$ heterojunction phototransistors grown by chemical beam epitaxy," *IEEE Electron Dev. Lett.*, vol. EDL-8, pp. 171-173, 1987.
[11] O. Wada, H. Nobuhara, H. Hamaguchi, T. Mikawa, A. Tackeuchi, and T. Fujii, "Very high speed InGaAs metal-semiconductor-metal photodiode incorporating and AlInAs GaInAs graded superlattice," *Appl. Phys. Lett.*, vol. 54, pp. 16-17, 1989.
[12] J. B. D. Soole, H. Schumacher, H. P. Leblanc, R. Bhat, and M. A. Koza, *IEEE Photon. Technol. Lett.*, vol. 1, pp. 250-252, 1989.
[13] M. S. Ünlü, K. Kishino, J. I. Chyi, J. Reed, S. Noor Mohammad, and H. Morkoç, "Resonant cavity enhanced AlGaAs/GaAs heterojunction phototransistors with an intermediate InGaAs region in the collector," *Appl. Phys. Lett.*, vol. 57, pp. 750-752, 1990.
[14] A. Chin and T. Y. Chang, "Multilayer reflectors by molecular beam epitaxy for resonance enhanced absorption in thin high-speed detectors," *J. Vac. Sci. Technol.*, vol. 8, pp. 339-342, 1990.
[15] H. Ishio, J. Minowa, and K. Nusu, "Review and status of wavelength-division-multiplexing technology," *J. Lightwave Technol.*, vol. LT-2, pp. 448-463, 1984.
[16] Y. Suematsu, S. Arai, and K. Kishino, *J. Lightwave Technol.*, vol. LT-1, pp. 161-176, 1983.
[17] R. H. Yan, R. J. Simes, and L. A. Coldren, "Analysis and design of surface-normal Fabry-Perot electrooptic modulators," *IEEE J. Quantum Electron.*, vol. 25, pp. 2272-2280, 1989.
[18] J. E. Bowers and C. A. Burrus, "Ultrawide-band long- wavelength p-i-n photodetectors," *J. Lightwave Technol.*, vol. LT-5, pp. 1339-1350, 1987.
[19] H. Uetsuka, N. Kurosawa, and K. Imoto, "Novel method of center wavelength tuning of silica waveguide type Mach-Zender multi/demultiplexers," *Electron. Lett.*, vol. 26, pp. 251-253, 1990.
[20] T. Baba, S. Tamura, Y. Kokubun, and S. Watanabe, "Monolithic integration of multilayer filter on vertical surface of semiconductor substrate by a bias-sputtering technique," *IEEE Photon. Technol. Lett.*, vol. 2, pp. 191-193, 1990.
[21] A. Larsson, P. A. Anderkson, P. Andersson, S. T. Eng, J. Salzman, and A. Yariv, "High-speed dual-wavelength demultiplexing and detection in a monolithic superlattice p-i-n waveguide detector array," *Appl. Phys. Lett.*, vol. 49, pp. 233-235, 1986.
[22] H. Takahashi, S. Suzuki, K. Kato, and I. Nishi, "Arrayed-waveguide grating for wavelength division multi/demultiplexer with nanometer resolution," *Electron. Lett.*, vol. 26, pp. 87-88, 1990.
[23] M. S. Ünlü, K. Kishino, J. I. Chyi, L. Arsenault, J. Reed, and H. Morkoç, "Wavelength demultiplexing heterojunction phototransistors," *Electron. Lett.*, vol. 26, pp. 1857-1858, 1990.

Katsumi Kishino (M'88), photograph and biography not available at the time of publication.

M. Selim Ünlü (S'90) was born in Sinop, Turkey, in 1964. He received the B.S. degree in electrical engineering from Middle East Technical University, Ankara, Turkey, in 1986 and the M.S.E.E. degree from the University of Illinois, Urbana, in 1988.

He is currently working toward the Ph.D. degree in electrical engineering at the University of Illinois. From 1984 to 1986, he was a part-time research engineer at the Military Electronics Inc., Ankara, Turkey, where he worked on VHF communication systems. His current research interests include the fabrication, characterization, and modeling of semiconductor electronic and opto-electronic devices.

Jen-Inn Chyi received the B.S.E.E. and M.S.E.E. degrees from National Tsing Hau University, Hsinchu, Taiwan, R.O.C., in 1982 and 1984, respectively. He received the Ph.D. degree from the University of Illinois in 1990. His dissertation topic dealt with molecular beam epitaxial growth and characterization of InSb on GaAs.

He is currently with the Department of Electrical Engineering, National Central University, Chung-Li, Taiwan, R.O.C. He has authored or coauthored some 35 technical journal articles.

Dr. Chyi is a member of Phi Tau Phi Scholastic Honor Society.

J. Reed, photograph and biography not available at the time of publication.

L. Arsenault, photograph and biography not available at the time of publication.

Hadis Morkoç (S'72-M'76-SM'79-F'87) received the B.S.E.E. and M.S.E.E. degrees from Istanbul Technical University, Turkey, in 1968 and 1969, respectively. He began his Ph.D. studies at Michigan State University in 1971 and later transferred to Cornell University where he received the Ph.D. degree in electrical engineering in 1975. His dissertation topic dealt with liquid phase epitaxy of GaAs FET's.

He was with Varian Associates, Palo Alto, CA, from 1976 to 1978, where he was heavily involved in various novel FET structures. He has held visiting positions at AT&T Bell Laboratories (1978-1979), the California Institute of Technology, and the Jet Propulsion Laboratory (1987-1988). Since 1978, he has been with the University of Illinois pursuing research in heterostructure devices and materials. He has authored, coauthored, or edited *Principles and Technology of MODFETs*, 10 book chapters and proceedings, some 600 technical journal articles, 100 conference papers, and 40 technical reports. He has served as a consultant to some 15 industrial laboratories.

Dr. Morkoç is a Fellow of the American Association for the Advancement of Science, a Fellow of the American Physical Society, a member of the Material Research Society, a member of the Optical Society of America, a life member of Sigma Xi, a member of Eta Kappa Nu, and a life member of Phi Kappa Phi. He is listed in Who's in the Midwest American Men and Women in Science, Who's Who in Engineering, and International Men of Achievement. He received the ELECTRONIC LETTERS Best Paper award in 1978 for his work in InGaAs FET's.